Editors' Suggestion | Featured in Physics

Interacting-Bath Dynamical Embedding for Capturing Nonlocal Electron Correlation in Solids

Jiachen Li and Tianyu Zhu*
Department of Chemistry, Yale University, New Haven, Connecticut 06520, USA

(Received 14 July 2024; accepted 25 September 2024; published 20 November 2024)

Quantitative simulation of electronic structure of solids requires treating local and nonlocal electron correlations on an equal footing. We present a new *ab initio* formulation of Green's function embedding which, unlike dynamical mean-field theory that uses noninteracting bath, derives bath representation with general two-particle interactions in a systematically improvable manner. The resulting interacting-bath dynamical embedding theory (ibDET) utilizes an efficient real-axis coupled-cluster solver to compute the self-energy, approaching the full system limit at much reduced cost. When combined with the *GW* theory, GW + ibDET achieves good agreement with experimental spectral properties across a range of semiconducting, insulating, and metallic materials. Our approach also enables quantifying the role of nonlocal electron correlation in determining material properties and addressing the long-standing debate on the bandwidth narrowing of metallic sodium.

DOI: 10.1103/PhysRevLett.133.216402

Introduction—Predictive description of material-specific electronic properties remains a significant challenge in computational physics and chemistry [1]. The main reason is the need for quantitative treatment of electron correlation effects and simulating in the thermodynamic limit simultaneously. Quantum embedding theories offer a promising route to solve this problem [2]. For dynamical quantities, dynamical mean-field theory (DMFT) has been the most popular choice, leading to advances in the understanding of correlated electron physics in lattice models and real materials [3–5].

Despite its success in treating strong local electron interactions, extending DMFT to accurately capture nonlocal electron correlation remains challenging [6]. This capability is crucial for describing various quantum many-body phenomena, such as the pseudogap phase and stripe orders in high-temperature cuprate superconductors [7–9]. Cluster extensions in real (cluster DMFT [10–12]) or reciprocal (DCA and DΓA [13–15]) spaces have been proposed, but these formalisms are mostly designed for short-range quantum fluctuations, and CDMFT is known to break translational invariance [16]. To account for band structure and long-range interactions in real materials, density functional theory (DFT) [17] or many-body perturbation theory (*GW*) [18–21] is normally adopted as the low-level theory for DMFT. Although much progress has been made in the downfolded DFT + DMFT [5] and GW + DMFT [22–25] formalisms, their predictive capability is limited by uncontrolled errors that are often difficult to quantify. The impurity problem usually comprises a few correlated orbitals, but DMFT results could depend sensitively on the choice and construction of these impurity orbitals [26]. The derivation of effective interactions and approximation to their frequency dependence also introduce numerical uncertainties [27]. Moreover, DFT + DMFT calculations could suffer from the double counting error [28,29].

To avoid these numerical ambiguities, one of us recently developed a full cell GW + DMFT formalism [30–32], where the impurity problem comprises all local orbitals of atoms within a chosen supercell. General bare Coulomb interactions within impurity orbitals are employed and solved by efficient quantum chemistry solvers [33,34], removing the need for downfolding. However, full cell GW + DMFT inevitably inherits certain limitations from cluster DMFT, such as the breaking of translational invariance. While the impurity space is significantly larger, the nonlocal electron correlation beyond the selected supercell is at best captured at the *GW* level. The neglect of long-range interactions stronger than those captured by *GW* is known to yield errors in a variety of settings [24,35].

A common origin of this challenge in DMFT is the *noninteracting* nature of its bath representation through the hybridization function. Despite a natural choice for continuous-time quantum Monte Carlo (CTQMC) solvers [36], the noninteracting bath parametrization does not fully leverage the power of Hamiltonian-based solvers, such as exact diagonalization (ED) [37], density matrix renormalization group (DMRG) [34,38], configuration interaction (CI) [39], and coupled-cluster (CC) theory [33,40–42], as there is no clear mapping between the full Hamiltonian and fictitious bath states. In this Letter, we develop a new *ab initio* Green's function embedding formulation with

*Contact author: tianyu.zhu@yale.edu

interacting bath, which enables direct projection of the full interacting Hamiltonian into large embedding problems, solved by a coupled-cluster Green's function (CCGF) solver truncated at the single-reference singles and doubles level [33]. Unlike DMFT, this formulation utilizes self-energy corrections to both impurity and bath states for describing dynamical quantities, allowing the computation of coupled-cluster spectra at substantially reduced cost. Because we do not derive bath parameters by fitting the hybridization function, this method is, strictly speaking, no longer DMFT, and we term it interacting-bath dynamical embedding theory (ibDET).

Method—Given a periodic crystal, we start with a mean-field solution at the Hartree-Fock (HF) or DFT level using crystalline Gaussian atomic orbitals. To define the impurity problem, we construct the orthogonal atom-centered local orbital basis employing an intrinsic atomic orbital plus projected atomic orbital (IAO + PAO) scheme [43,44]. We choose all local orbitals on a single atom as the impurity and then gradually expand the bath space by selecting orbitals that entangle most strongly with impurity orbitals from the environment. To recover the self-energy of the full crystal, multiple embedding problems need to be formulated, each centered on an impurity atom in the unit cell.

The key step is then to perform algebraic construction of bath orbitals that allow projection from full Hamiltonian to the embedding space (Fig. 1). Here, we construct bath orbitals responsible for capturing short- and long-range electron correlations, respectively. The *first* set B_{DM} is derived by a Schmidt decomposition, i.e., using the singular value decomposition (SVD) of the mean-field off-diagonal one-particle reduced density matrix (1-RDM) between the impurity and remaining lattice [44], the same as in density matrix embedding theory [45]. B_{DM} ensures that impurity 1-RDM is exactly reproduced in the embedding calculation at the mean-field level [46]. The *second* set B_{GF} is obtained by performing SVD of the imaginary part of mean-field off-diagonal Green's function $g(\omega_n)$ on a uniform real-frequency grid, to capture the frequency-dependent entanglement between impurity and environment [52], a role similar to that of the hybridization function in DMFT. To keep the number of B_{DM} and B_{GF} orbitals tractable, we couple bath orbitals only to valence impurity orbitals (i.e., IAOs) and adopt an additional projection to orthogonalize the embedding space and remove redundant B_{GF} orbitals. B_{DM} and B_{GF}, however, do not capture electron correlation beyond short range, so we derive a *third* set of cluster-specific natural bath orbitals B_{NO} inspired by local correlation methods in quantum chemistry, particularly the local natural orbital coupled-cluster (LNO-CC) theory [53]. Similar idea was recently introduced to quantum embedding by Nusspickel and Booth [54] and periodic CC theory [55] for ground-state properties. The key is to select natural orbitals from the environment that correlate strongly to the existing embedding cluster ($I \bigoplus B_{\mathrm{DM}} \bigoplus B_{\mathrm{GF}}$, where I stands for the impurity space), estimated by a cheap direct second-order perturbation theory (dMP2) calculation. Furthermore, to better describe the delocalized conduction states in gapped systems, we incorporate a few low-lying canonical virtual orbitals into the bath space [46].

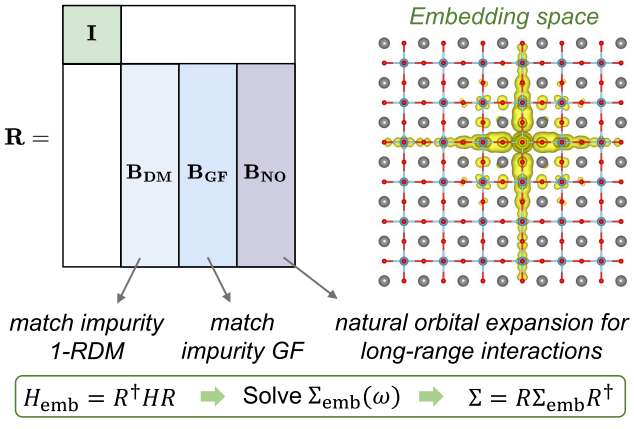

FIG. 1. Illustration of the ibDET formalism, where each embedding space includes all local orbitals of an impurity atom (I) in the unit cell coupled to large interacting bath (B). An example of an occupied embedding space in $SrTiO_3$ (Ti as impurity) is shown.

The Hamiltonian for each embedding problem is

$$H_{\mathrm{emb}} = \sum_{ij}^{\mathrm{emb}} \tilde{F}_{ij} a_i^\dagger a_j + \frac{1}{2} \sum_{ijkl}^{\mathrm{emb}} (ij|kl) a_i^\dagger a_k^\dagger a_l a_j, \qquad (1)$$

where $(ij|kl)$ is the general two-particle bare Coulomb interaction matrix defined on all impurity and bath orbitals, obtained through a projection with rotation matrix R (see Fig. 1 for the definition of R). The one-particle interaction matrix is defined as

$$\tilde{F}_{ij} = F_{ij}^{\mathrm{emb}} - \sum_{kl}^{\mathrm{emb}} \gamma_{kl}^{\mathrm{emb}} \left[(ij|lk) - \frac{1}{2} (ik|lj) \right]. \qquad (2)$$

Here, $F^{\mathrm{emb}} = R^\dagger F^{\mathrm{full}} R$, where F^{full} is the Fock matrix of the full system computed using HF (even when we start from the DFT density), and γ^{emb} is the 1-RDM rotated to the embedding space. The HF contribution to the self-energy is exactly removed in Eq. (2), so there is no double counting in ibDET.

The CCGF solver at the EOM-CCSD level [33] is adopted to solve the embedding Hamiltonians [Eq. (1)] on the real axis. We choose the CCGF solver because of its good performance for various lattice models and real materials [56–60], as well as high computational efficiency. Meanwhile, we emphasize that ibDET can utilize any Hamiltonian-based solvers, such as quantum chemistry DMRG [38] and selected configuration interaction [61]

that are more robust for stronger correlation. The self-energy computed within the embedding space is rotated back to the full Hilbert space

$$\Sigma^{\mathrm{full},J}(\omega) = R\Sigma^{\mathrm{emb},J}(\omega)R^{\dagger}, \tag{3}$$

where J means the Jth embedding problem. The self-energy matrices $\{\Sigma^{\mathrm{full},J}(\omega)\}$ from all embedding calculations are then assembled using a democratic partitioning scheme and Fourier transformed to the momentum space, to obtain the full self-energy of the crystal $\Sigma^{\mathrm{ibDET}}(\mathbf{k},\omega)$. Similar to $GW+\mathrm{DMFT}$, ibDET can be easily combined with the GW theory to capture any small long-range correlation effects missed by ibDET, and the resulting $GW+\mathrm{ibDET}$ self-energy is

$$\Sigma^{GW+\mathrm{ibDET}} = \Sigma^{GW,\mathrm{full}} + \Sigma^{\mathrm{CC,ibDET}} - \Sigma^{GW,\mathrm{ibDET}}, \tag{4}$$

where $\Sigma^{GW,\mathrm{full}}$ is the GW self-energy of the full system. Different from common DFT + DMFT and $GW+\mathrm{DMFT}$ calculations that require self-consistency, all results in this Letter are obtained from one-shot ibDET.

Results—We first demonstrate numerical convergence of ibDET results on silicon (Si) and two-dimensional hexagonal boron nitride (2D BN), where full EOM-CCSD calculations are possible. For Si and 2D BN, GTH-cc-pVTZ/GTH-DZVP basis sets [62,63] and GTH-HF-rev/GTH-PADE pseudopotentials [64,65] were employed, together with $4\times4\times4/6\times6\times1$ $\mathbf{k}$-point sampling. For Si, it is not feasible to run full EOM-CCSD calculation, thus we used a composite correction scheme [66] to estimate band gaps. All calculations were conducted using the PYSCF quantum chemistry software package [67,68].

In Fig. 2(a), we show the convergence of $GW+\mathrm{ibDET}$ predictions of silicon band gaps against the full system

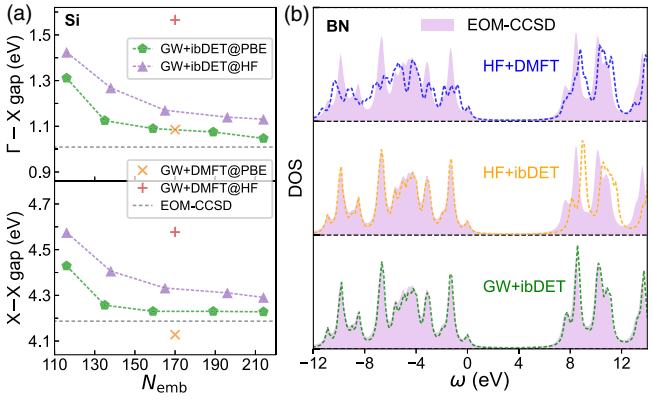

FIG. 2. Benchmark of ibDET on Si and 2D BN against EOM-CCSD. (a) Convergence of $GW+\mathrm{ibDET}$ band gaps of Si as the number of embedding orbitals is increased, compared to full cell $GW+\mathrm{DMFT}$ values [30]. (b) DOS of 2D BN from HF + ibDET and $GW+\mathrm{ibDET}$ (HF reference), compared to the HF + DMFT spectrum [31].

limit, which is challenging for quantum embedding methods due to the long-range nature of the screened interaction [30,31,69]. Although one-shot G_0W_0 approximation on top of PBE [70] predicts accurate band structure for Si, this success benefits from error cancellations, indicated by the large difference between G_0W_0@PBE (1.15 eV) and G_0W_0@HF (1.86 eV) Γ-X band gaps. The $GW+\mathrm{ibDET}$ predicted band gaps quickly converge to the full EOM-CCSD limit as the embedding space grows. At around 210 embedding orbitals (6% of the total number of orbitals, N_{tot}), the $GW+\mathrm{ibDET}$ (PBE reference) Γ-X and X-X band gap errors are both only 0.04 eV. Furthermore, since the long-range electron correlation is mostly captured by the CCGF solver within ibDET, the starting-point dependence is significantly reduced from 0.71 to 0.08 eV (Γ-X gap) when using PBE vs. HF reference, which is also smaller than in full cell $GW+\mathrm{DMFT}$ with similar embedding size (0.48 eV, $N_{\mathrm{emb}}=170$).

ibDET also predicts accurate photoemission spectrum on 2D BN [Fig. 2(b)]. Previous full cell HF + DMFT simulation with a BN unit cell as the impurity yields accurate band gaps, but the spectrum shape shows some discrepancies, especially in the valence part [31], an indication of broken translational symmetry. In contrast, the density of states (DOS) predicted by HF + ibDET (200 orbitals in each embedding space) is in good agreement with full EOM-CCSD, suggesting the treatment of nonlocal electron correlation is substantially improved and the translational symmetry is preserved. The valence spectrum is near perfect, although the band gap is overestimated due to the large error in HF. $GW+\mathrm{ibDET}$ (HF reference) further improves over HF + ibDET and achieves quantitative agreement with EOM-CCSD over a wide frequency range.

We then apply $GW+\mathrm{ibDET}$ to study two metal oxides (MgO and $SrTiO_3$) with large $\mathbf{k}$-point sampling ($6\times6\times6$) impossible for standard EOM-CCSD implementation. MgO has an experimental band gap of 7.98–8.19 eV [66,71], but G_0W_0@PBE underestimates the band gap (7.43 eV [20]) and quasiparticle self-consistent GW largely overestimates (9.33 eV [21]). We performed $GW+\mathrm{ibDET}$ (PBE reference) calculation using all-electron cc-pVTZ basis set, with 230 orbitals in each embedding space (2% of N_{tot}). As presented in Fig. 3(a) and Table S6, $GW+\mathrm{ibDET}$ greatly improves over G_0W_0@PBE and predicts the band gap to be 8.22 eV, which is also consistent with recent EOM-CCSD benchmark (8.34 eV [66]).

For the moderately correlated insulator $SrTiO_3$, the experimental indirect band gap is 3.25 eV [72]. Although $SrTiO_3$ has no open-shell $3d$ electrons, its lowest conduction bands are dominated by localized Ti-$3d$ orbitals, causing severe underestimation of the band gap by PBE (1.82 eV). G_0W_0@PBE overestimates the band gap (3.62 eV), while various self-consistent GW schemes yield even larger overestimation errors [73,74]. We conducted $GW+\mathrm{ibDET}$ calculations using

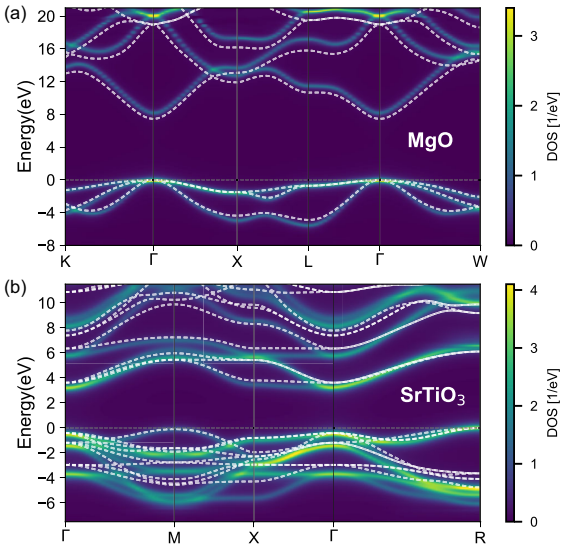

FIG. 3. Band structure of MgO and $SrTiO_3$ computed by $GW +$ ibDET (heat map) and G_0W_0@PBE (white dashes).

all-electron def2-TZVP/def2-SVP basis sets [75] for Ti and O, and GTH-DZVP-MOLOPT-SR/GTH-HF-rev basis/pseudopotential for Sr. As seen in Fig. 3(b) and Table S7, with around 210 orbitals in each embedding space (1% of N_{tot}), $GW +$ ibDET (PBE reference) predicts the R-Γ and Γ-Γ band gaps to be 3.24 and 3.74 eV, in excellent agreement with experimental values. Comparing the G_0W_0@PBE and $GW +$ ibDET band structures, we find that $GW +$ ibDET predicts broader valence band spectrum due to the shift of O-dominant peaks by 1–2 eV.

Finally, we demonstrate the applicability of ibDET to metallic systems, using sodium (Na) as an example. Although Na is usually considered as near-free-electron weakly correlated, DFT with LDA or GGA functionals severely overestimates the occupied bandwidth of Na (e.g., 3.41 eV from PBE) compared to those measured by angle-resolved photoemission spectroscopy (ARPES) experiments (2.65–2.78 eV) [76,77], which leads to long-standing debate over the nature of electron correlation in Na [24,78–82]. Adding nonlocal static exchange in hybrid functionals yields even worse results [79]. The GW approximation is also insufficient, as G_0W_0 only slightly improves over LDA and GGA (e.g., G_0W_0@PBE value is 3.20 eV). Single-site DFT + DMFT and self-consistent $GW +$ EDMFT have been applied to this problem, where the impurity is a single Na-3s orbital. LDA + eDMFT predicted a bandwidth of 2.84 eV [79], which resulted in the conclusion that only local electron correlation within single Na atom needs to be captured beyond DFT. However, Ref. [24] showed contradictory result (3.2–3.3 eV, no improvement over GW) from $GW+$ EDMFT, which suggested treating Na-Na nonlocal correlation beyond GW is important. Such discrepancy is likely due to the use of different effective interaction parameters within the downfolding scheme.

We thus apply ibDET, which is free of downfolding parameters and treats significantly larger embedding space (225 orbitals), to address this puzzle. The CCGF solver was previously shown to agree well with DMRG on the spectral function of a small uniform electron gas model at the relevant Wigner-Seitz radius $r_s = 4$ [78]. Our $GW +$ ibDET (PBE reference) simulation employed GTH-cc-pVTZ basis set [62] and GTH-HF-rev pseudopotential and $8 \times 8 \times 8$ $\mathbf{k}$-mesh. In Fig. 4(a), we find that $GW +$ ibDET achieves excellent agreement with the ARPES spectra [76,77] and predicts an occupied bandwidth of 2.84 eV, significantly better than G_0W_0@PBE and PBE.

Now that we have established the accuracy of $GW +$ ibDET, we further analyze the nature of electron correlation in metallic sodium. Specifically, we ask if the same good bandwidth prediction can be obtained

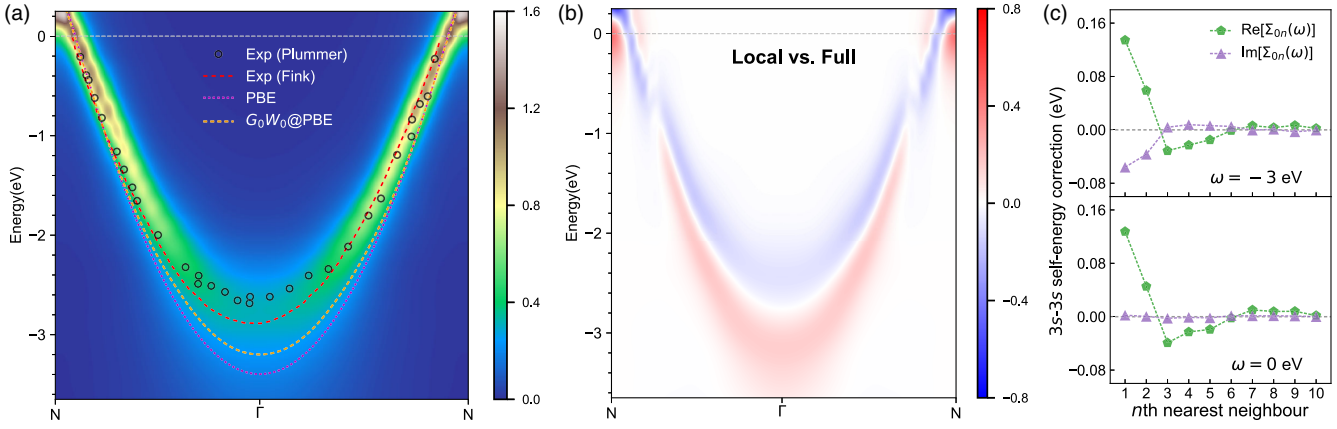

FIG. 4. $GW +$ ibDET results for metallic sodium. (a) Band structure computed by $GW +$ ibDET (heat map), compared against PBE, G_0W_0@PBE, and ARPES experiments by Plummer [76] and Fink [77]. (b) DOS(Local) − DOS(Full), computed by applying self-energy correction ($\Sigma^{\mathrm{CC}} - \Sigma^{GW}$) to the full system (Full) or only to the diagonal block within each Na atom (Local). (c) 3s-3s nonlocal self-energy correction ($\Sigma^{\mathrm{CC}} - \Sigma^{GW}$) between Na atoms as the Na-Na distance increases.

with only local self-energy approximation, by limiting the $\Sigma^{CC} - \Sigma^{GW}$ self-energy correction to the diagonal block within each Na atom (this approximation is similar to single-site DFT + DMFT and GW + EDMFT). In Fig. 4(b), we find that, without nonlocal interatomic self-energy correction beyond GW, the bandwidth predicted by "local" GW + ibDET is 3.11 eV, only slightly improved over G_0W_0@PBE (3.20 eV) and much worse than that predicted by full GW + ibDET (2.84 eV). Furthermore, GW + ibDET allows us to quantify the magnitude of real-space long-range electron correlation. In Fig. 4(c), we find that the real part of interatomic $3s$-$3s$ self-energy correction ($\Sigma^{CC} - \Sigma^{GW}$) does not decay to zero until 6th nearest neighbor in distance, indicating the electron correlation is quite delocalized in metallic sodium. Thus, to quantitatively simulate spectral properties of sodium, we argue it is crucial to account for long-range electron correlation at a many-body level beyond DFT and GW, as seen in GW + ibDET.

Conclusion—We have developed a new Green's function embedding formulation, interacting-bath dynamical embedding theory, for capturing local and nonlocal electron correlations on an equal footing in many-body simulation of solids. The main strength of this method is that it avoids uncontrolled errors associated with small impurity subspace and empirical truncations, while fully leveraging the power of advanced quantum chemistry solvers for treating long-range electron correlation effects. We have demonstrated that the GW + ibDET approach achieves quantitative description of spectral properties across a wide range of materials and preserves the translational invariance. In particular, ibDET provides a capability to examine the effect of nonlocal (and even long-range) electron correlation in determining material-specific electronic properties. GW + ibDET is thus a promising tool for tackling material problems in which nonlocal electron correlation plays a significant role.

Acknowledgments—This work was supported by the National Science Foundation under Grant No. CHE-2337991 and a start-up fund from Yale University. J. L. also acknowledges support from the Tony Massini Postdoctoral Fellowship in Data Science from Yale University.

[1] P. R. Kent and G. Kotliar, Toward a predictive theory of correlated materials, Science **361**, 348 (2018).
[2] Q. Sun and G. K.-L. Chan, Quantum embedding theories, Acc. Chem. Res. **49**, 2705 (2016).
[3] A. Georges and G. Kotliar, Hubbard model in infinite dimensions, Phys. Rev. B **45**, 6479 (1992).
[4] A. Georges, G. Kotliar, W. Krauth, and M. J. Rozenberg, Dynamical mean-field theory of strongly correlated fermion systems and the limit of infinite dimensions, Rev. Mod. Phys. **68**, 13 (1996).
[5] G. Kotliar, S. Y. Savrasov, K. Haule, V. S. Oudovenko, O. Parcollet, and C. A. Marianetti, Electronic structure calculations with dynamical mean-field theory, Rev. Mod. Phys. **78**, 865 (2006).
[6] G. Rohringer, H. Hafermann, A. Toschi, A. A. Katanin, A. E. Antipov, M. I. Katsnelson, A. I. Lichtenstein, A. N. Rubtsov, and K. Held, Diagrammatic routes to nonlocal correlations beyond dynamical mean field theory, Rev. Mod. Phys. **90**, 025003 (2018).
[7] M. Hashimoto, I. M. Vishik, R.-H. He, T. P. Devereaux, and Z.-X. Shen, Energy gaps in high-transition-temperature cuprate superconductors, Nat. Phys. **10**, 483 (2014).
[8] B. X. Zheng, C. M. Chung, P. Corboz, G. Ehlers, M. P. Qin, R. M. Noack, H. Shi, S. R. White, S. Zhang, and G. K. L. Chan, Stripe order in the underdoped region of the two-dimensional Hubbard model, Science **358**, 1155 (2017).
[9] H. Xu, C. M. Chung, M. Qin, U. Schollwöck, S. R. White, and S. Zhang, Coexistence of superconductivity with partially filled stripes in the Hubbard model, Science **384**, eadh7691 (2024).
[10] A. I. Lichtenstein and M. I. Katsnelson, Antiferromagnetism and d-wave superconductivity in cuprates: A cluster dynamical mean-field theory, Phys. Rev. B **62**, R9283 (2000).
[11] G. Kotliar, S. Y. Savrasov, G. Pálsson, and G. Biroli, Cellular dynamical mean field approach to strongly correlated systems, Phys. Rev. Lett. **87**, 186401 (2001).
[12] G. Biroli and G. Kotliar, Cluster methods for strongly correlated electron systems, Phys. Rev. B **65**, 155112 (2002).
[13] M. H. Hettler, A. N. Tahvildar-Zadeh, M. Jarrell, T. Pruschke, and H. R. Krishnamurthy, Nonlocal dynamical correlations of strongly interacting electron systems, Phys. Rev. B **58**, R7475 (1998).
[14] T. A. Maier, M. Jarrell, T. Pruschke, and M. Hettler, Quantum cluster theories, Rev. Mod. Phys. **77**, 1027 (2005).
[15] A. Toschi, A. A. Katanin, and K. Held, Dynamical vertex approximation: A step beyond dynamical mean-field theory, Phys. Rev. B **75**, 045118 (2007).
[16] M. Klett, N. Wentzell, T. Schäfer, F. Simkovic, O. Parcollet, S. Andergassen, and P. Hansmann, Real-space cluster dynamical mean-field theory: Center-focused extrapolation on the one- and two particle-levels, Phys. Rev. Res. **2**, 033476 (2020).
[17] W. Kohn and L. J. Sham, Self-consistent equations including exchange and correlation effects, Phys. Rev. **140**, A1133 (1965).
[18] M. S. Hybertsen and S. G. Louie, Electron correlation in semiconductors and insulators: Band gaps and quasiparticle energies, Phys. Rev. B **34**, 5390 (1986).
[19] D. Golze, M. Dvorak, and P. Rinke, The GW compendium: A practical guide to theoretical photoemission spectroscopy, Front. Chem. **7**, 377 (2019).
[20] T. Zhu and G. K.-L. Chan, All-electron Gaussian-based G_0W_0 for valence and core excitation energies of periodic systems, J. Chem. Theory Comput. **17**, 727 (2021).
[21] J. Lei and T. Zhu, Gaussian-based quasiparticle self-consistent GW for periodic systems, J. Chem. Phys. **157**, 214114 (2022).
[22] P. Sun and G. Kotliar, Extended dynamical mean-field theory and GW method, Phys. Rev. B **66**, 085120 (2002).

[23] S. Biermann, F. Aryasetiawan, and A. Georges, First-principles approach to the electronic structure of strongly correlated systems: Combining the *GW* approximation and dynamical mean-field theory, Phys. Rev. Lett. **90**, 086402 (2003).
[24] F. Nilsson, L. Boehnke, P. Werner, and F. Aryasetiawan, Multitier self-consistent $GW + \mathrm{EDMFT}$, Phys. Rev. Mater. **1**, 043803 (2017).
[25] J. Tomczak, P. Liu, A. Toschi, G. Kresse, and K. Held, Merging GW with DMFT and non-local correlations beyond, Eur. Phys. J. Spec. Top. **226**, 2565 (2017).
[26] J. Karp, A. Hampel, and A. J. Millis, Dependence of $\mathrm{DFT} + \mathrm{DMFT}$ results on the construction of the correlated orbitals, Phys. Rev. B **103**, 195101 (2021).
[27] F. Aryasetiawan, M. Imada, A. Georges, G. Kotliar, S. Biermann, and A. I. Lichtenstein, Frequency-dependent local interactions and low-energy effective models from electronic structure calculations, Phys. Rev. B **70**, 195104 (2004).
[28] X. Wang, M. J. Han, L. de' Medici, H. Park, C. A. Marianetti, and A. J. Millis, Covalency, double-counting, and the metal-insulator phase diagram in transition metal oxides, Phys. Rev. B **86**, 195136 (2012).
[29] L. Muechler, D. I. Badrtdinov, A. Hampel, J. Cano, M. Rösner, and C. E. Dreyer, Quantum embedding methods for correlated excited states of point defects: Case studies and challenges, Phys. Rev. B **105**, 235104 (2022).
[30] T. Zhu and G. K.-L. Chan, *Ab initio* full cell $GW + \mathrm{DMFT}$ for correlated materials, Phys. Rev. X **11**, 021006 (2021).
[31] T. Zhu, Z.-H. Cui, and G. K.-L. Chan, Efficient formulation of *ab initio* quantum embedding in periodic systems: Dynamical mean-field theory, J. Chem. Theory Comput. **16**, 141 (2020).
[32] T. Zhu, L. Peng, H. Zhai, Z.-H. Cui, and G. K.-L. Chan, Towards an exact electronic quantum many-body treatment of Kondo correlation in magnetic impurities, arXiv:2405.18709.
[33] T. Zhu, C. A. Jiménez-Hoyos, J. McClain, T. C. Berkelbach, and G. K.-L. Chan, Coupled-cluster impurity solvers for dynamical mean-field theory, Phys. Rev. B **100**, 115154 (2019).
[34] E. Ronca, Z. Li, C. A. Jimenez-Hoyos, and G. K.-L. Chan, Time-step targeting time-dependent and dynamical density matrix renormalization group algorithms with *ab initio* Hamiltonians, J. Chem. Theory Comput. **13**, 5560 (2017).
[35] A. L. Kutepov, Spatial non-locality of electronic correlations beyond GW approximation, J. Phys. Condens. Matter **33**, 485601 (2021).
[36] E. Gull, A. J. Millis, A. I. Lichtenstein, A. N. Rubtsov, M. Troyer, and P. Werner, Continuous-time Monte Carlo methods for quantum impurity models, Rev. Mod. Phys. **83**, 349 (2011).
[37] A. Liebsch and H. Ishida, Temperature and bath size in exact diagonalization dynamical mean field theory, J. Phys. Condens. Matter **24**, 053201 (2012).
[38] H. Zhai, H. R. Larsson, S. Lee, Z. H. Cui, T. Zhu, C. Sun, L. Peng, R. Peng, K. Liao, J. Tölle, J. Yang, S. Li, and G. K. L. Chan, Block2: A comprehensive open source framework to develop and apply state-of-the-art DMRG algorithms in electronic structure and beyond, J. Chem. Phys. **159**, 234801 (2023).
[39] D. Zgid, E. Gull, and G. K.-L. Chan, Truncated configuration interaction expansions as solvers for correlated quantum impurity models and dynamical mean-field theory, Phys. Rev. B **86**, 165128 (2012).
[40] M. Nooijen and J. G. Snijders, Coupled cluster Green's function method: Working equations and applications, Int. J. Quantum Chem. **48**, 15 (1993).
[41] B. Peng and K. Kowalski, Green's function coupled-cluster approach: Simulating photoelectron spectra for realistic molecular systems, J. Chem. Theory Comput. **14**, 4335 (2018).
[42] A. Shee and D. Zgid, Coupled cluster as an impurity solver for Green's function embedding methods, J. Chem. Theory Comput. **15**, 6010 (2019).
[43] G. Knizia, Intrinsic atomic orbitals: An unbiased bridge between quantum theory and chemical concepts, J. Chem. Theory Comput. **9**, 4834 (2013).
[44] Z.-H. Cui, T. Zhu, and G. K.-L. Chan, Efficient implementation of *ab initio* quantum embedding in periodic systems: Density matrix embedding theory, J. Chem. Theory Comput. **16**, 119 (2020).
[45] G. Knizia and G. K.-L. Chan, Density matrix embedding: A simple alternative to dynamical mean-field theory, Phys. Rev. Lett. **109**, 186404 (2012).
[46] See Supplemental Material at http://link.aps.org/supplemental/10.1103/PhysRevLett.133.216402 for details of constructing bath orbitals B_{DM}, which includes Refs. [44,47–51].
[47] S. Wouters, C. A. Jiménez-Hoyos, Q. Sun, and G. K.-L. Chan, A practical guide to density matrix embedding theory in quantum chemistry, J. Chem. Theory Comput. **12**, 2706 (2016).
[48] F. Aquilante, T. K. Todorova, L. Gagliardi, T. B. Pedersen, and B. O. Roos, Systematic truncation of the virtual space in multiconfigurational perturbation theory, J. Chem. Phys. **131**, 034113 (2009).
[49] H. J. A. Jensen, P. Jorgensen, H. Ågren, and J. Olsen, Second-order moller-plesset perturbation theory as a configuration and orbital generator in multiconfiguration self-consistent field calculations, J. Chem. Phys. **88**, 3834 (1988).
[50] D. Mester, P. R. Nagy, and M. Kállay, Reduced-cost linear-response CC2 method based on natural orbitals and natural auxiliary functions, J. Chem. Phys. **146**, 194102 (2017).
[51] B. T. G. Lau, B. Busemeyer, and T. C. Berkelbach, Optical properties of defects in solids via quantum embedding with good active space orbitals, J. Phys. Chem. C **128**, 2959 (2024).
[52] M. Nusspickel and G. H. Booth, Efficient compression of the environment of an open quantum system, Phys. Rev. B **102**, 165107 (2020).
[53] Z. Rolik and M. Kllay, A general-order local coupled-cluster method based on the cluster-in-molecule approach, J. Chem. Phys. **135**, 104111 (2011).
[54] M. Nusspickel and G. H. Booth, Systematic improvability in quantum embedding for real materials, Phys. Rev. X **12**, 011046 (2022).

[55] H.-Z. Ye and T. C. Berkelbach, Periodic local coupled-cluster theory for insulators and metals, arXiv:2407.11258.
[56] J. McClain, Q. Sun, G. K.-L. Chan, and T. C. Berkelbach, Gaussian-based coupled-cluster theory for the ground-state and band structure of solids, J. Chem. Theory Comput. **13**, 1209 (2017).
[57] K. Laughon, J. M. Yu, and T. Zhu, Periodic coupled-cluster Green's function for photoemission spectra of realistic solids, J. Phys. Chem. Lett. **13**, 9122 (2022).
[58] T. Gruber, K. Liao, T. Tsatsoulis, F. Hummel, and A. Grüneis, Applying the coupled-cluster ansatz to solids and surfaces in the thermodynamic limit, Phys. Rev. X **8**, 021043 (2018).
[59] T. N. Mihm, T. Schäfer, S. K. Ramadugu, L. Weiler, A. Grüneis, and J. J. Shepherd, A shortcut to the thermodynamic limit for quantum many-body calculations of metals, Nat. Comput. Sci. **1**, 801 (2021).
[60] X. Xing and L. Lin, Inverse volume scaling of finite-size error in periodic coupled cluster theory, Phys. Rev. X **14**, 011059 (2024).
[61] S. Sharma, A. A. Holmes, G. Jeanmairet, A. Alavi, and C. J. Umrigar, Semistochastic heat-bath configuration interaction method: Selected configuration interaction with semistochastic perturbation theory, J. Chem. Theory Comput. **13**, 1595 (2017).
[62] H.-Z. Ye and T. C. Berkelbach, Correlation-consistent Gaussian basis sets for solids made simple, J. Chem. Theory Comput. **18**, 1595 (2022).
[63] J. VandeVondele, M. Krack, F. Mohamed, M. Parrinello, T. Chassaing, and J. Hutter, Quickstep: Fast and accurate density functional calculations using a mixed Gaussian and plane waves approach, Comput. Phys. Commun. **167**, 103 (2005).
[64] C. Hartwigsen, S. Goedecker, and J. Hutter, Relativistic separable dual-space Gaussian pseudopotentials from H to Rn, Phys. Rev. B **58**, 3641 (1998).
[65] S. Goedecker, M. Teter, and J. Hutter, Separable dual-space Gaussian pseudopotentials, Phys. Rev. B **54**, 1703 (1996).
[66] E. A. Vo, X. Wang, and T. C. Berkelbach, Performance of periodic EOM-CCSD for bandgaps of inorganic semiconductors and insulators, J. Chem. Phys. **160**, 044106 (2024).
[67] Q. Sun, T. C. Berkelbach, N. S. Blunt, G. H. Booth, S. Guo, Z. Li, J. Liu, J. D. McClain, E. R. Sayfutyarova, S. Sharma, S. Wouters, and G. K. L. Chan, PYSCF: The PYTHON-based simulations of chemistry framework, Comput. Mol. Sci. **8**, e1340 (2018).
[68] Q. Sun *et al.*, Recent developments in the PYSCF program package, J. Chem. Phys. **153**, 024109 (2020).
[69] W. Chibani, X. Ren, M. Scheffler, and P. Rinke, Self-consistent Green's function embedding for advanced electronic structure methods based on a dynamical mean-field concept, Phys. Rev. B **93**, 165106 (2016).
[70] J. P. Perdew, K. Burke, and M. Ernzerhof, Generalized gradient approximation made simple, Phys. Rev. Lett. **77**, 3865 (1996).
[71] X. Ren, F. Merz, H. Jiang, Y. Yao, M. Rampp, H. Lederer, V. Blum, and M. Scheffler, All-electron periodic G_0W_0 implementation with numerical atomic orbital basis functions: Algorithm and benchmarks, Phys. Rev. Mater. **5**, 013807 (2021).
[72] K. van Benthem, C. Elsässer, and R. H. French, Bulk electronic structure of $SrTiO_3$: Experiment and theory, J. Appl. Phys. **90**, 6156 (2001).
[73] G. Kang, Y. Kang, and S. Han, Influence of wave-function updates in *GW* calculations on titanates, Phys. Rev. B **91**, 155141 (2015).
[74] C. Bhandari, M. van Schilfgaarde, T. Kotani, and W. R. L. Lambrecht, All-electron quasiparticle self-consistent *GW* band structures for $SrTiO_3$ including lattice polarization corrections in different phases, Phys. Rev. Mater. **2**, 013807 (2018).
[75] F. Weigend and R. Ahlrichs, Balanced basis sets of split valence, triple zeta valence and quadruple zeta valence quality for H to Rn: Design and assessment of accuracy, Phys. Chem. Chem. Phys. **7**, 3297 (2005).
[76] I.-W. Lyo and E. W. Plummer, Quasiparticle band structure of Na and simple metals, Phys. Rev. Lett. **60**, 1558 (1988).
[77] D. V. Potorochin, R. Kurleto, O. J. Clark, E. D. L. Rienks, J. Sánchez-Barriga, F. Roth, V. Voroshnin, A. Fedorov, W. Eberhardt, B. Büchner, and J. Fink, Lifetime of quasiparticles in the nearly free electron metal sodium, Phys. Rev. B **106**, 125138 (2022).
[78] J. McClain, J. Lischner, T. Watson, D. A. Matthews, E. Ronca, S. G. Louie, T. C. Berkelbach, and G. K.-L. Chan, Spectral functions of the uniform electron gas via coupled-cluster theory and comparison to the *GW* and related approximations, Phys. Rev. B **93**, 235139 (2016).
[79] S. Mandal, K. Haule, K. M. Rabe, and D. Vanderbilt, Electronic correlation in nearly free electron metals with beyond-DFT methods, npj Comput. Mater. **8**, 1 (2022).
[80] J. S. Zhou, M. Gatti, J. J. Kas, J. J. Rehr, and L. Reining, Cumulant Green's function calculations of plasmon satellites in bulk sodium: Influence of screening and the crystal environment, Phys. Rev. B **97**, 035137 (2018).
[81] L. Craco and S. Leoni, LDA+DMFT approach to electronic structure of sodium metal, Phys. Rev. B **100**, 115156 (2019).
[82] J. Lischner, T. Bazhirov, A. H. MacDonald, M. L. Cohen, and S. G. Louie, Effect of spin fluctuations on quasiparticle excitations: First-principles theory and application to sodium and lithium, Phys. Rev. B **89**, 081108(R) (2014).